Aging of the (2 + 1)-dimensional Kardar-Parisi-Zhang model

Géza Ódor,[1] Jeffrey Kelling,[2,3] and Sibylle Gemming[2,3]

[1]*MTA TTK MFA Research Institute for Natural Sciences, P. O. Box 49, H-1525 Budapest, Hungary*

[2]*Institute of Ion Beam Physics and Materials Research Helmholtz-Zentrum, Dresden-Rossendorf,*
P. O. Box 51 01 19, 01314 Dresden, Germany

[3]*Institute of Physics, TU Chemnitz 09107 Chemnitz, Germany*

Extended dynamical simulations have been performed on a (2 + 1)-dimensional driven dimer lattice-gas model to estimate aging properties. The autocorrelation and the autoresponse functions are determined and the corresponding scaling exponents are tabulated. Since this model can be mapped onto the (2 + 1)-dimensional Kardar-Parisi-Zhang surface growth model, our results contribute to the understanding of the universality class of that basic system.

I. INTRODUCTION

Physical aging occurring in different systems such as glasses, polymers, reaction-diffusion systems, or cross-linked networks has been studied in physics systematically [1]. Aging occurs naturally in irreversible systems, relaxing towards nonequilibrium stationary states (for a recent comprehensive overview, see [2]). In many systems a single dynamical length scale $L(t) \sim t^{1/z}$ describes the dynamics out of equilibrium [3], where z is the dynamical exponent. In aging systems the time-translation invariance is broken and they are best characterized by two-time quantities, such as the dynamical correlation and response functions [4]. The dynamical scaling laws and exponents describing these functions characterize the nonequilibrium universality classes [5].

In the aging regime, $s \gg \tau_m$ and $t - s \gg \tau_m$, where τ_m is a microscopic time scale, one expects the following laws for autocorrelation $[C(t,s)]$ and autoresponse $[R(t,s)]$ functions of the field ϕ:

$$C(t,s) = \langle \phi(t)\phi(s) \rangle - \langle \phi(t) \rangle \langle \phi(s) \rangle = s^{-b} f_C\left(\frac{t}{s}\right),$$

$$R(t,s) = \left.\frac{\delta \langle \phi(t) \rangle}{\delta j(s)}\right|_{j=0} = \langle \phi(t)\widetilde{\phi}(s) \rangle = s^{-1-a} f_R\left(\frac{t}{s}\right), \quad (1)$$

where s denotes the start and $t > s$ the observation time, and j is the external conjugate to ϕ. These laws include the so-called aging exponents a,b and the scaling functions, with the asymptotic behavior $f_{C,R}(t/s) \sim (t/s)^{-\lambda_{C,R}/z}$ and the autocorrelation and autoresponse exponents $\lambda_{C,R}$. In non-Markovian systems they can be independent, but symmetries can relate them to each other via scaling laws (see [2,5]).

The Kardar-Parisi-Zhang (KPZ) equation describes the evolution of a fundamental nonequilibrium model and exhibits aging behavior. The state variable is the height function $h(\mathbf{x},t)$ in the d-dimensional space

$$\partial_t h(\mathbf{x},t) = v + \nu \nabla^2 h(\mathbf{x},t) + \lambda [\nabla h(\mathbf{x},t)]^2 + \eta(\mathbf{x},t). \quad (2)$$

Here v and λ are the amplitudes of the mean and local growth velocity, ν is a smoothing surface tension coefficient, and η roughens the surface by a zero-average, Gaussian noise field exhibiting the variance $\langle \eta(\mathbf{x},t)\eta(\mathbf{x}',t') \rangle = 2T\nu\delta^d(\mathbf{x} - \mathbf{x}')(t - t')$. The letter T is related to the noise amplitude (the temperature in the equilibrium system), d is the spatial dimensionality of the system, and $\langle \cdot \rangle$ denotes a distribution average.

Research on this nonlinear stochastic differential equation and the universality class introduced by Kardar, Parisi, and Zhang [6] is in the forefront of interest again nowadays. This is the consequence of emerging new techniques applied to the open questions [7–11] and experimental realizations [12]. This equation was inspired in part by the stochastic Burgers equation [13] and can describe the dynamics of simple growth processes in the thermodynamic limit [14], randomly stirred fluids [15], directed polymers in random media (DPRM) [16], dissipative transport [17,18], and the magnetic flux lines in superconductors [19]. In one dimension a mapping [20] onto the asymmetric exclusion process (ASEP) [21] exists. In this case the equation is solvable due to the Galilean symmetry [15] and an incidental fluctuation-dissipation symmetry [22].

It has been investigated by various analytical [7,23–27] and numerical methods [28–32]; still there are several controversial issues. Discretized versions of the KPZ equation have been studied a lot in the past decades [33–35]. Recently we have shown [36,37] that the mapping between the KPZ surface growth and the ASEP [20] can straightforwardly be extended to higher dimensions. In two dimensions the mapping is just the simple extension of the rooftop model to the octahedron model as can be seen on Fig. 1. The surface built up from octahedra can be described by the edges meeting in the up or down middle vertices. The up edges in the x or y directions are represented by the slopes $\sigma_{x/y} = 1$, and the down ones by $\sigma_{x/y} = -1$ in the model. This can also be understood as a special two-dimensional (2D) cellular automaton, with the generalized Kawasaki updating rules

$$\begin{pmatrix} -1 & 1 \\ -1 & 1 \end{pmatrix} \underset{q}{\overset{p}{\rightleftharpoons}} \begin{pmatrix} 1 & -1 \\ 1 & -1 \end{pmatrix} \quad (3)$$

with probability p for attachment and probability q for detachment. By the lattice-gas representation with $n_{x/y} = (1 - \sigma_{x/y})/2$ occupation variables, it describes the oriented migration of self-reconstructing dimers. We have confirmed that this mapping using the parametrization $\lambda = 2p/(p + q) - 1$ reproduces the one-point functions of the continuum model [36,37].
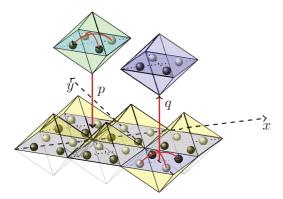
FIG. 1. (Color online) Mapping of the $(2 + 1)$-dimensional surface growth model (octahedra) on the 2D particle model (bullets). Detachment (probability p) and attachment (probability q) of octahedra correspond to Kawasaki exchanges of pairs of particles along the bisectrix of the x and y axes. The curved red arrows illustrate this as a superposition of two 1D processes. The 2D square lattice to be updated is given by the crossing points of the dotted lines.
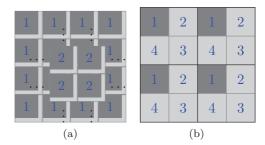

FIG. 2. (Color online) Sketches of the domain decomposition methods used to parallelize the model. Regions that can be updated independently at one time are filled dark grey. (a) Dead border scheme as used at device level. (b) Double tiling scheme as used at work-group level.

This kind of generalization of the ASEP model can be regarded as the simplest candidate for studying the KPZ equation in $d > 1$: a one-dimensional model of self-reconstructing d-mers on the d-dimensional space. Furthermore, this lattice gas can be studied by very efficient simulation methods. Dynamic, bit-coded simulations were run on extremely large-sized ($L \times L$) lattice-gas models [37,38], and the surface heights, reconstructed from the slopes

$$h_{i,j} = \sum_{l=1}^{i} \sigma_x(l,1) + \sum_{k=1}^{j} \sigma_y(i,k), \qquad (4)$$

were shown to exhibit KPZ surface growth scaling in $d = 1$–5 dimensions.

While aging in glassy systems follows a complex phenomenology [4], the dynamic renormalization group analysis of the KPZ model presented in [39] suggests that the one-scale dynamic scaling hypothesis is not spoiled for the KPZ universality class. This has been tested by simulation studies and the present work strengthens this view further.

Recently, in $(2 + 1)$ dimensions Daquila and Täuber [40] have simulated the long-time behavior of the density-density autocorrelation function of driven lattice gases [17] with particle exclusion and periodic boundary conditions in one to three spatial dimensions. In one dimension, their model is just the ASEP. They generalized this driven lattice-gas model to higher dimensions by keeping the ASEP dynamics in one of the dimensions and performing unbiased random walk(s) in the orthogonal dimension(s). In two dimensions they reported $\lambda_C/z = 1$ and $b = -1$. We will show here that our generalization of the ASEP model, which exhibits the surface growth scaling of the $(2 + 1)$-dimensional KPZ model provides different autocorrelation exponents.

Even more recently, Henkel *et al.* [41] have determined the following aging exponents of the $(1 + 1)$-dimensional KPZ equation: $a = -1/3$, $b = -2/3$, $\lambda_C = \lambda_R = 1$, and $z = 3/2$. They solved the discretized KPZ equation (2) in the strong-coupling limit [42] or else the Kim-Kosterlitz (KK) model [43]. The KK model uses a height variable $h_i(t) \in \mathbb{Z}$ attached

to the sites of a chain with L sites and subject to the constraints $|h_i(t) - h_{i\pm 1}(t)| = 0,1$, at all sites i.

II. BIT-CODED GRAPHICS PROCESSING UNIT ALGORITHMS

The height of each surface site is thoroughly determined by two slopes, along the x and y axes, respectively, whose absolute values are restricted to unity. Thus at each site two bits of information are required; hence a chunk of 4×4 sites is encoded in one 32-bit word.

Two different layers of parallelization are used that reflect the two-layered computing architecture provided by graphics processing units (GPUs) [44]: noncommunicating blocks at *device level* and communicating threads at *work-group level*. Parallelization of the algorithm is enabled by splitting the system into spatial domains, which can be updated independently for a limited time without introducing relevant errors. At the device layer a domain decomposition scheme using dead borders is employed; see Fig. 2(a). Here conflicts at the subsystem borders are avoided by not updating them. A random translation is applied to the origin of the decomposition periodically. These translations are restricted to multiples of four sites, because 4×4 sites are encoded in one 32-bit word. At work-group level a *double tiling* decomposition is employed; see Fig. 2(b). Here the tiles assigned to different work items are split into 2^d domains. In our two-dimensional problem, this creates 2^2 sets of noninteracting domains, each set consisting of one domain out of every tile. The active set of domains is randomly chosen before each update.

For random number generation, each thread uses a 64-bit linear congruential generator. The threads skip ahead in the sequence, in order to take numbers from disjunct sub-sequences [45].

A more detailed description of our CUDA implementation can be found in [46,47]. For this work we added the capability to perform simulations with arbitrary probabilities p and q. Benchmarks, comparing our GPU implementation on a Tesla C2070 to the optimized sequential CPU implementation running on an Intel Xeon X5650 at 2.67 GHz, have shown a speedup factor of about 230 for the raw simulation. The basic version from [47], which contains less computational effort per update, reaches a raw simulation speedup of about 100, in the same setup.

We decided not to implement space-dependent disorder in our GPU code, because we need this code only for the very small fraction of the computation before the waiting time $s \leqslant 100$ Monte Carlo steps. Thus the projected benefit regarding time-to-solution would not have justified the effort. Simulations to obtain autoresponse calculations were performed using the CPU code up to the waiting time and then continued on the GPU. The overall speedup factor obtained by using a GPU in our case was about 17. The difference from the number stated above results from using the CPU code until the waiting time is reached and, predominantly, from the computation of the autoresponse not being done in parallel. In the autocorrelation runs measurements were performed asynchronously with the simulation, in both CPU and GPU versions. For these runs the gross speedup from using a GPU is about 50.

Applying any kind of domain decomposition to a stochastic cellular automaton introduces an error. This error is kept small by keeping the ratio between the volume of domains and the number of updated sites between synchronization events large as well as by conserving the equidistribution of site selection as well as possible. The validity of the results was checked primarily by comparing with results obtained with the sequential CPU implementation. For the autocorrelation of slopes we noticed possible signs of saturation below $C_n \lesssim 1 \times 10^{-4}$. This gives an upper limit for the accuracy of our GPU results, independent of statistics. Further investigations suggest that the above-mentioned restriction of the translations of the decomposition origin to multiples of four sites may be the sole source of this error. This restriction impairs the equidistribution of site selection, while not enough to measurably change the W^2 scaling, enough to visibly change the autocorrelation behavior of the system. We assume that this problem can be taken care of by removing this restriction in the future.

III. AGING SIMULATIONS

We have run simulations for linear sizes $L = 2^{12}, 2^{13}, 2^{15}$ of independent sample numbers $40\,000, 30\,000, 2000$ (respectively), by starting from half-filled (striped) lattice gases. The time between measurements increases exponentially

$$t_{i+1} = (t_i + 10) \times e^m, \quad \text{with} \quad m > 0, \quad t_0 = 0, \quad (5)$$

when the program calculates the heights $h_{\vec{r}}$ via Eq. (4) at each lattice site $\vec{r} = (i, j)$ and writes out the autocorrelation and the autoresponse values to files, which are analyzed later. We used $s = 30, 100, 300$ start times in the two-point function measurements. By simple scaling the morphology of the surface is characterized by the roughness

$$W^2(L,t) = \frac{1}{L^2} \sum_{\vec{r}}^{L^2} \langle [h_{\vec{r}}(t) - \overline{h}(t)]^2 \rangle \quad (6)$$

on a lattice with L^2 sites and average height $\overline{h}(t) = L^{-2} \sum_{\vec{r}} h_{\vec{r}}(t)$, which obeys the scaling relation

$$W(L,t) = L^\alpha f(t L^{-z}), \quad f(u) \sim \begin{cases} u^\beta & \text{for } u \ll 1, \\ \text{const} & \text{for } u \gg 1. \end{cases} \quad (7)$$
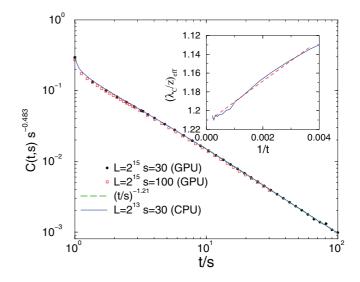

FIG. 3. (Color online) Autocorrelation function scaling of the height variables for $L = 2^{15}$, $s = 30$ (bullets) and $s = 100$ (squares) and $L = 2^{13}$, $s = 30$ (line). The dashed line shows a power-law fit for $t/s > 10$ with the slope -1.21. Inset: Local slopes of the $L = 2^{13}$, $s = 30$ data defined as (9). The dashed line shows a power-law fit.

In this form β is the growth exponent and the roughness exponent is $\alpha = \beta z$. Throughout this paper we used the estimates from our previous high-precision simulation study [38]: $\alpha = 0.393(4)$, $\beta = 0.2415(15)$, and the dynamical scaling exponent $z = \alpha/\beta = 1.627(26)$.

Similarly to the one-dimensional case we considered here the two-time temporal correlator

$$\begin{aligned} C(t,s) &= \langle [h(t;\vec{r}) - \langle \overline{h}(t;\vec{r}) \rangle][h(s;\vec{r}) - \langle \overline{h};\vec{r}(s) \rangle] \rangle \\ &= \langle h(t;\vec{r})h(s;\vec{r}) \rangle - \langle \overline{h}(t;\vec{r}) \rangle \langle \overline{h}(s;\vec{r}) \rangle \\ &= s^{-b} f_C\left(\frac{t}{s}\right), \end{aligned} \quad (8)$$

were $\langle \cdot \rangle$ denotes averaging over sites and independent runs. The autocorrelation exponent can be read off in the $(t/s) \to \infty$ limit, $f_C(t/s) \sim (t/s)^{-\lambda_C/z}$, and since $W^2(t; \infty) = C(t,t) = t^{-b} f_C(1)$ the $b = -2\beta$ relation holds. The simulations were tested by blocking the communication in one of the directions and comparing the results with those of the one-dimensional KPZ aging results [41]. As we found a perfect match we assume that our two-dimensional results give reliable numerical estimates.

As Fig. 3 shows we could obtain remarkable data collapse for $s = 30$ and $s = 100$ by simulating $(2^{15} \times 2^{15})$-sized systems on GPUs. Throughout this paper all quantities plotted are dimensionless. For smaller sizes it is more difficult to reach a regime of large t/s, due to the low signal-to-noise ratio. We performed careful correction-to-scaling analysis by calculating the local slopes of the autocorrelation function exponents for $t \to \infty$. The effective exponents can be estimated similarly as in the cases of other scaling laws [5] as the discretized, logarithmic derivative

$$(\lambda/z)_{\text{eff}}(t_i) = \frac{\ln C(t_i) - \ln C(t_{i+1})}{\ln(t_{i+1}) - \ln(t_i)}, \quad (9)$$

and we extrapolated to the asymptotic behavior with the form

$$(\lambda/z)_{\text{eff}}(t_i) = \lambda/z + at^x \tag{10}$$

for $t > 250$. On the inset of Fig. 3 one can see a roughly linear approach as $1/t \to 0$ with $\lambda_C/z = 1.21(1)$ and $a = 20$. However, periodic corrections to scaling can also be observed, which are the consequence of density fluctuations being transported through a finite system by kinematic waves [37,48].

This provides $\lambda_C = 1.97(3)$, in marginal agreement with the $\lambda_C = d$ conjecture of [49], based on a purely geometric argument. In [39] a $(2 + 1)$-dimensional ballistic deposition model of linear size $L = 240$ and $t \leqslant 1000$ was simulated. Scaling with the form $C_L(t,s) \propto (t/s)^{-1.65(5)}$ is reported, which is out of the error margin of our large-scale simulations and of the scaling law $\lambda_C/z = (d + 4)/z - 2 \simeq 1.08(5)$ derived in [39].

We have also calculated the autocorrelation of the density variables

$$\begin{aligned} C_n(t,s) &= \langle [n(t;\vec{r}) - \langle \bar{n}(t;\vec{r}) \rangle][n(s;\vec{r}) - \langle \bar{n};\vec{r}(s) \rangle] \rangle \\ &= \langle n(t;\vec{r})n(s;\vec{r}) \rangle - \langle \bar{n}(t;\vec{r}) \rangle \langle \bar{n}(t;\vec{r}) \rangle \\ &= s^{-b'} f_C'\left(\frac{t}{s}\right); \end{aligned} \tag{11}$$

however, that decays much faster than the height autocorrelator and obtaining a reasonable signal-to-noise ratio requires much higher statistics. This constrained the maximum time we could reach. Still, as Fig. 4 shows, good data collapse could be achieved with $b' = -0.70(1)$ and $C_n(s,t) \propto (t/s)^{-2.35(2)}$ asymptotically. In fact the height-height and the density-density correlation functions can be related, since we have a one-dimensional motion of dimers, for which the authors of
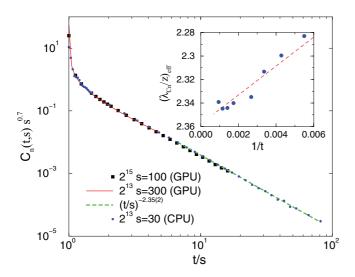
[50] derived

$$C_n(r,t) \sim \frac{\partial^2}{\partial r^2} C(r,t). \tag{12}$$

Indeed, a $2/z \simeq 1.23$ difference seems to connect the measured autocorrelator exponents $\lambda_C/z = 1.21(1)$ and $\lambda_{C_n}/z = 2.35(2)$ fairly well.

Next, we investigated the scaling of the autoresponse function in a similar way as described in [41]. Initially we applied a space-dependent deposition rate $p_i = p_0 + a_i \varepsilon/2$ with $\Delta = \pm 1$ and $\varepsilon = 0.005$ a small parameter. Then later on we used the same stochastic noise η (random sequences), in two realizations. System A evolved, up to the waiting time s, with the site-dependent deposition rate p_i and afterwards with the uniform deposition rate $p_0 = (1 - q_0) = 0.98$. System B evolved always with the uniform deposition rate $p_i = p_0$. The time-integrated response function is

$$\begin{aligned} \chi(t,s) &= \int_0^s du \, R(t,u) \\ &= \frac{1}{L^2} \sum_{\vec{r}}^{L^2} \left\langle \frac{h_{\vec{r}}^{(A)}(t,s) - h_{\vec{r}}^{(B)}(t)}{\varepsilon \Delta} \right\rangle = s^{-a} f_\chi\left(\frac{t}{s}\right). \end{aligned} \tag{13}$$

Asymptotically for $(t/s) \to \infty$ one can read off the autoresponse exponent $f_\chi(y) \sim (t/s)^{-\lambda_R/z}$.

Again, first we tested our programs by comparing the results against the one-dimensional KPZ case [41] by restricting the communication among particles to one of the directions. Then we run large-scale simulations on CPUs for $L = 2^{13}$ up to 30 000 samples and for GPUs for $L = 2^{13}$ up to 37 000 samples. Hardware independence was confirmed and a good scaling collapse was achieved by the exponents shown on Fig. 5. We performed local slope analysis similarly as in case of the autocorrelations (9). A least-squares error power-law
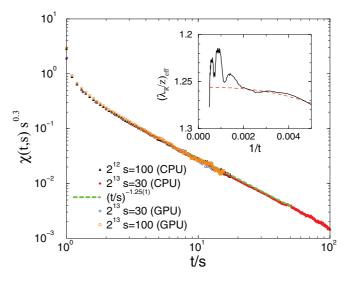

FIG. 4. (Color online) Autocorrelation function scaling of the lattice-gas variables for $L = 2^{15}$, $s = 100$ (boxes, GPU), $L = 2^{13}$, $s = 300$ (line, GPU), and $L = 2^{13}$, $s = 30$ (squares, CPU). The dashed line shows a power-law fit $\sim(t/s)^{-2.35(2)}$ for $t/s > 4$. Inset: Local slopes of the $L = 2^{13}$, $s = 30$ data defined as (9). The dashed line shows a power-law fit.

FIG. 5. (Color online) Autoresponse function scaling for $L = 2^{12}$ (CPU), $s = 100$, triangles, and $s = 30$, dots, and $L = 2^{13}$ (GPU), $s = 30$, circles, and $s = 100$, squares. The dashed line shows an asymptotic fit $\sim(t/s)^{1.25(1)}$ for the $L = 2^{13}$, $s = 30$ data in the $10 < t/s < 50$ region. Inset: Local slopes of the $L = 2^{13}$, $s = 30$ data defined as (9). The dashed line shows a power-law fit.

TABLE I. Scaling exponents of the $d = (2+1)$-dimensional KPZ class.

a	b	λ_R	λ_C	β	α
0.30(1)	$-0.483(2)$	2.04(3)	1.97(3)	0.2415(15)	0.393(4)

fitting (10) resulted in a roughly quadratic approach to the asymptotics $\lambda_R/z = 1.255(10) - 200t^2$ as shown in the inset of Fig. 5. Corrections to the long-time scaling are stronger and they suggest oscillating convergence as in the case of the autocorrelations. Most obvious is that $\lambda_R \neq \lambda_C$, so the fluctuation-dissipation relation $TR(t,s) = -\partial_r^2 C(t,s)$, which is fulfilled in one dimension due to the time-reversal symmetry [15,27,51], is broken here. The aging exponents are different from those of the 1D KPZ model [41] and those of the 2D driven lattice-gas model of [40]. They are summarized in Table I.

IV. CONCLUSIONS AND DISCUSSION

We have extended our previous, bit-coded 2D driven dimer lattice-gas model simulations with autocorrelation and autoresponse measurement capability in order to investigate the aging behavior. This gas can be mapped onto a surface growth (octahedron) model, which exhibits KPZ surface scaling exponents; thus our height autocorrelation and autoresponse functions describe the aging properties of two-dimensional KPZ surfaces. By performing extensive simulations on both CPUs and GPUs we have determined the aging exponents for this universality class. The autocorrelation exponents are different from those of the two-dimensional driven lattice gas [40] and of the simulations of [39]; however, fairly good agreement was found with the hypothesis of [49]. Weak violation of the fluctuation-dissipation relation is confirmed numerically.

We have also provided numerical estimates for the autocorrelation exponents for the density variables of the dimer lattice gas. In one-dimensional models of self-reconstructing d-mers the conservation laws resulted in initial condition-dependent sectors, with different power laws [52,53], placing a question mark on the universality. In higher dimensions exclusion effects are less relevant [5]; furthermore, due to the KPZ surface mapping, not all initial conditions and particle configurations are allowed. Still, a more detailed study in this direction would be very interesting.

The performance of the GPU code with respect to the CPU algorithm is higher by about a factor of 230. Our method is capable of testing numerically the predictions of the local scale invariance hypothesis (see [2]) and is straightforwardly extendable to higher dimensions [37]. For $p = q$ in the octahedral adsorption-desorption model the long-time dynamics is governed by Edwards-Wilkinson scaling [36,54]. A numerical test of the aging properties with respect to analytical results is planned in a future work.

Note added. We recently learned that Halpin-Healy [55] obtained autocorrelation results for other different models: the restricted solid on solid model, the KPZ Euler model, and the DPRM model belonging to the KPZ class (for definitions, see [29]), which agree with ours provided an overall, model-dependent multiplication factor is applied.

[1] L. C. E. Struik, *Physical Aging in Amorphous Polymers and Other Materials* (Elsevier, New York, 1978).

[2] M. Henkel and M. Pleimling, *Non-Equilibrium Phase Transitions, Vol 2: Aging and Dynamical Scaling far from Equilibrium* (Springer, Heidelberg, 2010).

[3] A. J. Bray, Adv. Phys. **43**, 357 (1994).

[4] L. F. Cugliandolo, in *Slow Relaxation and Non-Equilibrium Dynamics in Condensed Matter*, edited by J.-L. Barrat, J. Dalibard, J. Kurchan, and M. V. Feigelman (Springer, Berlin, 2003).

[5] G. Ódor, *Universality in Nonequilibrium Lattice Systems* (World Scientific, Singapore, 2008).

[6] M. Kardar, G. Parisi, and Y.-C. Zhang, Phys. Rev. Lett. **56**, 889 (1986).

[7] T. Kloss, L. Canet, and N. Wschebor, Phys. Rev. E **86** 051124 (2012).

[8] I. Corwin, Random Matrices: Theory Appl. **01**, 1130001 (2012).

[9] T. Halpin-Healy, Phys. Rev. E **88**, 042118 (2013).

[10] J. Olejarz and P. L. Krapivsky, Phys. Rev. E **88**, 022109 (2013).

[11] M. Nicoli, R. Cuerno, and M. Castro, J. Stat. Mech.: Theory Exp. (2013) P11001.

[12] R. A. L. Almeida, S. O. Ferreira, T. J. Oliveira, and F. D. A. Aarão Reis, Phys. Rev. B **89**, 045309 (2014).

[13] J. M. Burgers, *The Nonlinear Diffusion Equation* (Riedel, Boston 1974).

[14] T. Halpin-Healy, Phys. Rev. A **42**, 711 (1990).

[15] D. Forster, D. R. Nelson, and M. J. Stephen, Phys. Rev. A **16**, 732 (1977).

[16] M. Kardar, Phys. Rev. Lett. **55**, 2923 (1985).

[17] M. Plischke and Z. Rácz, Phys. Rev. Lett. **54**, 2056 (1985).

[18] H. K. Janssen and B. Schmittmann, Z. Phys. B **63**, 517 (1986).

[19] T. Hwa, Phys. Rev. Lett. **69**, 1552 (1992).

[20] M. Plischke, Z. Rácz, and D. Liu, Phys. Rev. B **35**, 3485 (1987).

[21] H. Rost, Z. Wahrscheinlicheitstheor. Verwandte Geb. **58**, 41 (1981).

[22] M. Kardar, Nucl. Phys. B **290**, 582 (1987).

[23] M. Schwartz and S. F. Edwards, Europhys. Lett. **20**, 301 (1992).

[24] E. Frey and U. C. Täuber, Phys. Rev. E **50**, 1024 (1994).

[25] M. Lässig, Nucl. Phys. B **448**, 559 (1995).

[26] H. C. Fogedby, Phys. Rev. Lett. **94**, 195702 (2005).

[27] L. Canet, H. Chaté, B. Delamotte, and N. Wschebor, Phys. Rev. E **84**, 061128 (2011).

[28] B. M. Forrest and L. H. Tang, Phys. Rev. Lett. **64**, 1405 (1990).

[29] T. Halpin-Healy, Phys. Rev. Lett **109**, 170602 (2012).

[30] E. Marinari, A. Pagnani, and G. Parisi, J. Phys. A **33**, 8181 (2000).

[31] E. Marinari, A. Pagnani, G. Parisi, and Z. Rácz, Phys. Rev. E **65**, 026136 (2002).

[32] F. D. A. Aarão Reis, Phys. Rev. E **72**, 032601 (2005).

[33] P. Meakin, P. Ramanlal, L. M. Sander, and R. C. Ball, Phys. Rev. A **34**, 5091 (1986).

[34] A. L. Barabási and H. E. Stanley, *Fractal Concepts in Surface Growth* (Cambridge University Press, Cambridge 1995).

[35] J. Krug, Adv. Phys. **46**, 139 (1997).

[36] G. Ódor, B. Liedke, and K.-H. Heinig, Phys. Rev. E **79**, 021125 (2009).

[37] G. Ódor, B. Liedke, and K.-H. Heinig, Phys. Rev. E **81**, 031112 (2010).

[38] J. Kelling and G. Ódor, Phys. Rev. E **84**, 061150 (2011).

[39] M. Krech, Phys. Rev. E **55**, 668 (1997).

[40] G. L. Daquila and Uwe C. Täuber, Phys. Rev. E **83**, 051107 (2011).

[41] M. Henkel, J. D. Noh, and M. Pleimling, Phys. Rev. E **85**, 030102(R) (2012).

[42] T. J. Newman and M. R. Swift, Phys. Rev. Lett. **79**, 2261 (1997).

[43] J. M. Kim and J. M. Kosterlitz, Phys. Rev. Lett. **62**, 2289 (1989).

[44] NVIDIA CUDA Programming Guide, 3.1, 2010 (unpublished).

[45] M. Weigel, J. Comput. Phys. **231**, 3064 (2012).

[46] H. Schulz, Gergely Ódor, Géza Ódor, and Máté Ferenc Nagy, Comput. Phys. Commun. **182**, 1467 (2011).

[47] J. Kelling, G. Ódor, M. F. Nagy, H. Schulz, and K.-H. Heinig, Eur. Phys. J.: Spec. Top. **210**, 175 (2012).

[48] S. Gupta, S. N. Majumdar, C. Godréche, and M. Barma, Phys. Rev. E **76**, 021112 (2007).

[49] H. Kallabis and J. Krug, Europhys. Lett. **45**, 20 (1999).

[50] M. Prähofer and M. Spohn, *In and Out of Equilibrium*, Progress in Probability Vol. 51 (Birkhäuser, Boston, 2002), pp. 185–204.

[51] U. Deker and F. Haake, Phys. Rev. A **11**, 2043 (1975).

[52] G. I. Menon, M. Barma, and D. Dhar, J. Stat. Phys. **86**, 1237 (1997).

[53] M. Barma, M. D. Grynberg, and R. B. Stinchcombe, J. Phys.: Condens. Matter **19**, 065112 (2007).

[54] S. F. Edwards and D. R. Wilkinson, Proc. R. Soc. London, Ser. A **381**, 17 (1982)

[55] T. Halpin-Healy and G. Palasantzas, Europhys. Lett. **105**, 50001 (2014).